*Journal of Sound and Vibration* (1986) **105**(1), 151-167

# DE-DOPPLERIZATION AND ACOUSTIC IMAGING OF AIRCRAFT FLYOVER NOISE MEASUREMENTS†

G. P. HOWELL, A. J. BRADLEY, M. A. MCCORMICK AND J. D. BROWN
*Rolls-Royce Limited, P.O. Box* 31, *Derby DE*2 8*BJ, England*

(*Received* 21 *November* 1984, *and in revised form* 22 *March* 1985)

The technique described in this paper eliminates the Doppler effect from aircraft flyover noise measurements and generates narrow band spectra at required angles. Such a capability allows more accurate interpretation of flight data, and is necessary for a detailed comparison with predictions and static measurements, since $\frac{1}{3}$ octave or narrow band levels, before de-Dopplerization, yield limited information on tonal content. The paper first explains how a single microphone output is de-Dopplerized, and includes details of aircraft tracking and computer simulation of flyover measurements. The technique is especially relevant to the analysis of noise from counter-rotating propeller driven aircraft, and results are shown for an Avro Shackleton. It is also applied to a Boeing 757, with high bypass ratio turbofan engines. Narrow band spectra at selected angles, density plots of complete flyovers, and field shapes at constant frequencies are all presented. Acoustic imaging, achieved by focussing the de-Dopplerized signals from an array of microphones, is also described, and results from a Lockheed TriStar graphically illustrate its capability.

## 1. INTRODUCTION

In this paper we describe a technique for removing the Doppler effect of time compression and expansion due to source motion. We apply this to aircraft flyover noise measurements, and present the resulting narrow band spectral information in a variety of ways. In addition, we demonstrate how an acoustic image of the source can be constructed by summing the de-Dopplerized signals from an array of microphones.

One-third octave spectra yield little information either on the frequencies and levels of tones or on the character of the broad band noise. They are therefore inadequate for a detailed comparison with static data, a requirement which has become especially important with the possibility of static noise certification tests. Also, with the revived interest in propellers, accurate information on the tonal content of noise from propeller driven aircraft has become vital, so that reliable prediction methods can be developed.

Narrow band analysis (without de-Dopplerization) offers some improvement on $\frac{1}{3}$ octave levels, and some of the tones in the spectrum may become resolved. However, because of the Doppler effect, their frequencies are generally incorrect, and because this effect changes during the averaging time, they will be blurred. Complete de-Dopplerization, therefore, offers two distinct advantages: first, the tones become sharp, giving greater resolution, and secondly their frequencies are corrected, allowing positive identification. It then becomes possible, for example, to plot a field shape, showing the level of a particular tone as a function of emission angle. Finally, acoustic imaging allows the source strength to be plotted as a function of position for a particular frequency, and this can be of further assistance in understanding distributed or multiple sources.

† Presented at the Ninth AIAA/NASA Aeroacoustics Conference, Williamsburg, U.S.A., October 1984, as AIAA/NASA Paper No. 84-2355



0022-460X/86/040151+18 $03.00/0

Previous work along these lines has been limited. For example, although Roy [1] has given a formula for calculating Doppler frequency shifts for uniform source and receiver motion in a steady state medium, this does not assist in resolving and identifying tones. Verhas [2] has attempted to de-Dopplerize the noise from a Boeing 737 flyover, but the process is cumbersome and relies on guessing the track of the aircraft. Narrow band analysis and de-Dopplerization of flyover data have also been performed for both a simple acoustic source (Mueller and Preisser [3]) and a small turbofan engine (Preisser and Chestnutt [4]). Furthermore, in both these references results are compared with narrow band static data, and a description of the computer software is available [5]. However, the de-Dopplerization is performed simply by adjusting the frequency scale in the spectral domain: this does not eliminate the blurring of tones, caused by the continuously changing Doppler effect, although the result is improved to some extent by taking short averages and employing an ensemble-averaging technique with multiple microphones. Acoustic imaging in flight has not been attempted before, but the method adopted here follows a similar principle to that of the static acoustic telescope [6].

The de-Dopplerization technique described in this paper involves calculating the sequence of reception times corresponding to a particular set of regularly spaced emission times, for an assumed source position and velocity, and hence constructing an emission time history from the received signal. If the microphone is sampled at these reception times, then the Doppler effect is eliminated. Acoustic imaging is an extension of this process. If the de-Dopplerized signals from an array of several microphones are summed, the contributions from the assumed source position should reinforce whereas those from other positions should be suppressed; a scan of the source region can be constructed by repeating the process with different assumed source positions.

These techniques are explained in more detail in section 2.1, while the remainder of section 2 provides details of how they are put into practice. This includes a description of aircraft tracking and an overview of the computer programs involved, and it is also shown how flyover measurements can be simulated.

In section 3 results for both simulated and actual flyover data are discussed. The analysis of simulated data demonstrates how the signal to noise ratio depends on the initial digitization rate and on the method of interpolating between samples. Narrow band spectra at selected angles, density plots of complete flyovers, and field shapes at constant frequencies are presented for two aircraft. These are a Boeing 757, with high bypass ratio turbofan engines, and an Avro Shackleton with counter-rotating propellers. In both cases, de-Dopplerized narrow band spectra are essential for identifying tones and estimating their levels at various observation angles.

Finally, in section 4, we show some results of acoustic imaging. The value of flyover simulations is clearly demonstrated, while longitudinal and transverse scans for a Lockheed TriStar flyover graphically illustrate the capability of this technique.

## 2. TECHNIQUE

This section describes how de-Dopplerization and acoustic imaging are achieved in practice. In section 2.1 we explain the principles on which the techniques are based, giving details first of how the effects of time compression or expansion due to source motion are removed for each microphone and then how the outputs from an array of microphones are focussed. These processes depend on an accurate knowledge of the aircraft position relative to the observer as a function of time, and section 2.2 describes how the aircraft is tracked during each flyover. Section 2.3 summarizes the structure of the computer programs for initial digitization and subsequent analysis of the data. Finally,

in section 2.4, we mention the simulation of signals which would be received at the microphones by idealized sources in motion; this capability has proved invaluable, both in checking for errors in the analysis programs and also in understanding the behaviour of real data.

## 2.1. FUNDAMENTAL PRINCIPLES

The fundamental principle underlying the techniques described in this paper is that signals emitted by a moving source at evenly spaced time intervals are received by a stationary observer at irregularly spaced intervals. This is simply because the distance, and hence the propagation time, between the source and observer are continuously changing. De-Dopplerization of the received signal involves calculating the sequence of reception times which correspond to a particular set of equally spaced emission times. Hence one constructs a modified time history from the received signal in which the effects of time compression or expansion due to source motion have been removed. This time history may then be transformed to give an estimate of the de-Dopplerized power spectral density.

Consider, for example, the section of flight path between times $t_1$ and $t_2$, shown in Figure 1(a). During this time interval the aircraft starts at position $\mathbf{x}_0$ and flies with constant velocity $\mathbf{v}$, emitting signals at equally spaced intervals, $\Delta t$. (Symbols printed in bold face indicate three-dimensional vector quantities.) An array of microphones is set out on the ground at positions $\mathbf{m}_1$, $\mathbf{m}_2$, $\mathbf{m}_3$, and so on. The $n$th signal, emitted at time $t_1+(n-1)\Delta t$, is received by microphone $\mathbf{m}_j$ at time $\tau_{nj}$, given by

$$\tau_{nj} = t_1+(n-1)\,\Delta t+|\mathbf{x}_0+\mathbf{v}(n-1)\,\Delta t-\mathbf{m}_j|/c_0, \tag{1}$$

where $c_0$ is the speed of sound. Hence the signals received at the microphones are either compressed or expanded, as illustrated by Figure 1(b).

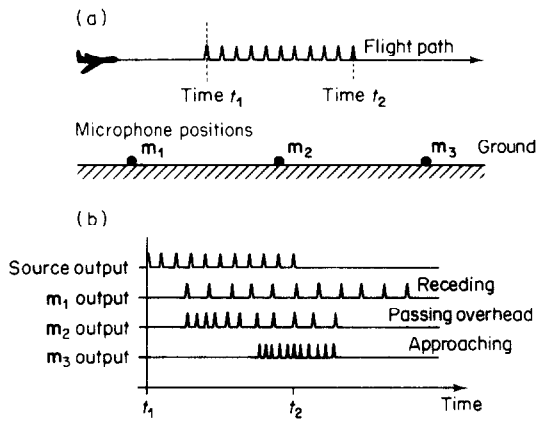


Figure 1. Illustration of the effects of source motion. (a) Signals are emitted at equally spaced time intervals by an aircraft flying over an array of three microphones; (b) the signals are received in a compressed or expanded form, after a time delay due to propagation time.

In practice, however, one requires a digital representation of the source output. Suppose, therefore, that the spikes in Figure 1 correspond to the times at which samples are required, rather than representing the source output itself. In this case $\Delta t$ is the time interval required between samples, and hence one must sample the microphone outputs at the times $\tau_{nj}$ given by equation (1). In general, since the outputs are digitized at regular

intervals, it is necessary to interpolate between individual samples, and the errors involved in this process are discussed in section 3.1.

As with all spectral analysis, the accuracy after transforming to the frequency domain depends on a trade-off between bandwidth and averaging time. Any improvement in the estimation of noise levels is at the expense of either a wider bandwidth or a longer averaging time. The latter is limited, however, in the case of flyover noise, by the emission angle resolution required. If acceptable bandwidth and accuracy cannot be achieved, then ensemble averaging techniques with multiple microphones can be employed to increase the averaging time without losing angular resolution. Such techniques have not been used in this work, but when investigating a tonal spectrum, a single transform is often sufficient to yield all the information required.

After de-Dopplerization, the time history will be correct only for the assumed source emission point. Furthermore, the approach involves the assumption that no reflected signals are present, since reflections can be viewed as apparent sources; this will not be a problem in this paper since all results are from ground level microphones. If an extended source becomes too large, however, it is impossible to de-Dopplerize accurately the output from a single microphone; this is because, for a given emission time, there is a range of reception times corresponding to emission from different parts of the source distribution. However, if the de-Dopplerized signals from an array of several microphones are summed, the contributions from the assumed source location should reinforce, whereas those from other locations will not have accurately realigned time histories and will therefore be supressed; the extent to which unwanted components are rejected in this way is discussed in section 4. The summed output can then be transformed to give an estimate of the power spectral density received from the assumed source position. The process can be repeated for a number of such assumed source positions, and hence the intensity distribution of the actual sources is constructed as a function of frequency and source position. Corrections for effects such as atmospheric absorption and ground impedance, which depend on the propagated (rather than de-Dopplerized) frequencies, can in principle be applied by digitally filtering the data before de-Dopplerization, although these are not included in the results presented in this paper. This form of acoustic imaging has been referred to as a "flyover acoustic telescope": the principle is similar to that of the static acoustic telescope [6], in which focussing also depends on accurately aligning the signals from an array of microphones, although in the flyover case such alignment is not possible until each signal has been de-Dopplerized.

### 2.2. AIRCRAFT TRACKING

It has been explained in the preceding section that de-Dopplerization and acoustic imaging both depend critically on an accurate knowledge of aircraft position relative to each microphone as a function of time. During each flyover, therefore, it is necessary that tracking information be recorded, on magnetic tape and camera film, and this must be processed before the acoustic data can be analyzed. Great care has been taken to ensure that the results are as accurate as possible.

A standard Hasselblad camera is attached to a tripod in such a way that it can be rotated to follow the aircraft, elevation and tilt angles being continuously encoded as sine wave frequencies in the range 4 to 8 kHz. The shutter is automatically opened and the film wound on at a rate a little faster than one photograph per second; the flash synchronization switch detects when the shutter is open and an electrical pulse is generated. The two sine wave signals and the camera pulses, together with the output from a time code generator (accurate to 1 ms), are recorded on four tracks of a tape recorder. The time code is also recorded alongside the acoustic data if a separate tape recorder is used.

Finally, the elevation and tilt angles are calibrated by recording the sine wave signals when the camera is moved to its extreme position in each direction, and the film is calibrated by photographing objects of measured separation at known distances from the camera.

To decode the angular information, one must estimate the frequencies of the two changing sine waves at the time of each pulse. This is done by digitizing the signals at a high rate (38 kHz) and then counting zero crossings. The "averaging time" for this process must be carefully chosen: if it is too short, accuracy will be lost, while if it is too long, the camera will have moved significantly during the average. An average of approximately 50 ms is normally used. The distance between aircraft and camera is estimated from a known dimension (for example, the separation of the wing tips) on each photograph, taking into account the elevation and tilt angles. In addition, corrections to the angles are calculated by measuring the displacement of the chosen aircraft tracking point (for example, the mid-point of the line joining the wing tips) from the centre of the photograph. These corrections are applied after conversion to the appropriate polar co-ordinates, and the corrected angles then allow one to make a more accurate estimate of distance.

Finally the co-ordinates are converted to Cartesian form, and each co-ordinate is plotted against time. A straight line is fitted to all the points which lie in the range 20° to 160° elevation on each graph, but a higher order polynomial may be used if necessary. Figures 2(a), (b) and (c) show these graphs for an Avro Shackleton aircraft flying at an altitude of approximately 440 ft and a speed of 250 ft/s. The typical accuracy of tracking is

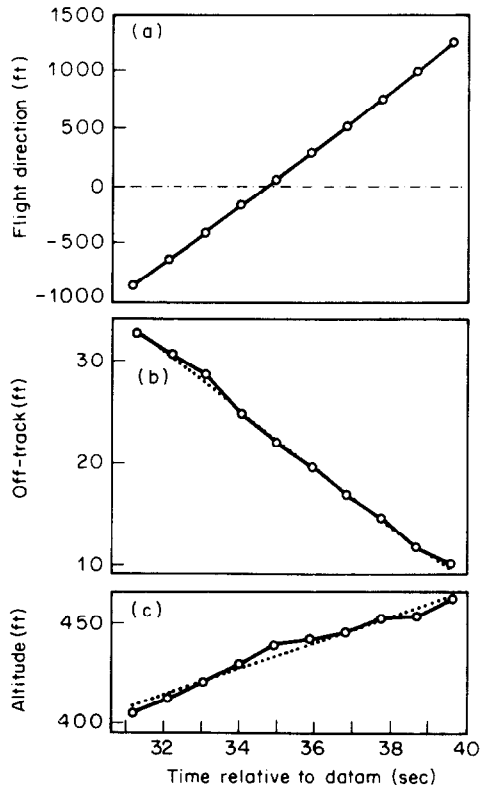


Figure 2. Tracking data for an Avro Shackleton flyover, in right-handed Cartesian co-ordinates relative to the camera position. O—O, Measured points; - - -, straight line fit to measured points.

demonstrated by the rms deviations from the fits, which are 7·1 ft (flight direction), 0·5 ft (off track) and 2·9 ft (altitude).

### 2.3. STRUCTURE OF COMPUTER PROGRAMS

The computing is done in two stages. First, digital samples are acquired from the analogue tape recording, and secondly these samples are de-Dopplerized, summed and transformed as required.

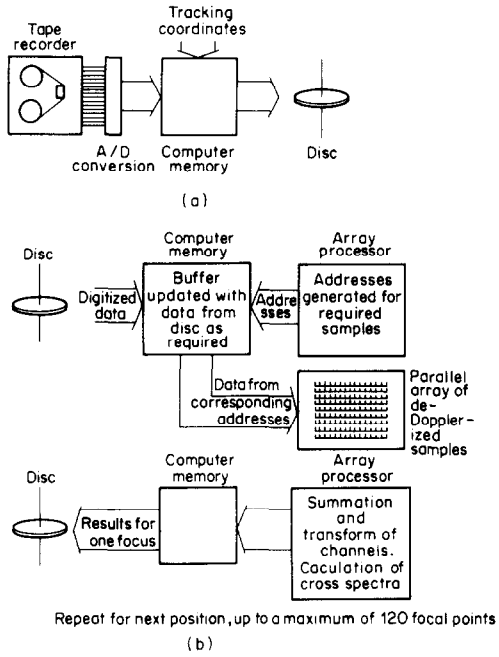


Figure 3. Schematic diagrams for computer programs. (a) Data acquisition from tape recorder; (b) data analysis for de-Dopplerization and acoustic imaging.

Figure 3(a) is a schematic representation of data acquisition. Up to 16 tape recorder channels can be digitized simultaneously, commencing at a specified time code. It is important that the digitization is continuous, with no samples being missed during the flyover, and for this reason the samples are double buffered in memory, allowing uninterrupted data transfer to disc. This requirement of continuity was found to restrict the digitization rate to 160 000 samples per second overall, with a maximum of 40 000 samples per second on each channel. Thus, for example, sixteen channels can be digitized simultaneously at more then 50 kHz if the tape speed is slowed down by a factor of 8 (e.g., 15 in./s to $1\frac{7}{8}$ in./s): in this case a total of 24 million half-word samples would be acquired from a 30 second flyover event. Alongside the data on disc are stored microphone positions and three-dimensional tracking co-ordinates of aircraft positions, with corresponding time codes.

The subsequent analysis is represented in Figure 3(b). Digitized samples on disc covering the required angle of emission are transferred back to the computer memory. An array processor, having calculated the addresses in memory of the samples required for interpolation, by using equation (1), builds up a parallel array of de-Dopplerized samples from whichever channels are required. These samples may then be summed and transformed to give a spectrum at one focus point of the telescope. The process is repeated for a range

of assumed source positions, relative to a fixed point on the aircraft; the focussed result may then be presented either as a scan of the source at a given frequency or as a spectrum at a particular source position. In addition, the phase of the cross spectrum, together with the coherence, between any pair of channels can be viewed in the same way. If acoustic imaging is not required, the array of de-Dopplerized samples in the array processor can be transformed to yield power spectra immediately: a separate computer program rapidly generates spectra both before and after de-Dopplerization over the whole flyover at given angular intervals.

### 2.4. SIMULATION OF FLYOVER MEASUREMENTS

As an alternative to the data acquisition described in the last section, it is possible to simulate the signals which would be received by an array of microphones from idealized sources in motion. In subsequent analysis the same computer programs as for real data are used.

The calculation of the received microphone signals is the inverse of the de-Dopplerizing procedure explained in section 2.1. Suppose the source moves with constant velocity $\mathbf{v}$, starting from position $\mathbf{x}_0$ at time $t=0$. Consider the sound emitted at time $t=t_e$ (from position $\mathbf{x}_0+\mathbf{v}t_e$) and received by a microphone (at position $\mathbf{m}$) at time $t=t_r$. The propagation time satisfies the relation

$$(t_r-t_e)=|\mathbf{x}_0+\mathbf{v}t_e-\mathbf{m}|/c_0, \tag{2}$$

where $c_0$ is the speed of sound. If one substitutes $\mathbf{x}=(\mathbf{x}_0-\mathbf{m})+\mathbf{v}t_r$, this becomes

$$(t_r-t_e)=|\mathbf{x}-\mathbf{v}(t_r-t_e)|/c_0. \tag{3}$$

Squaring this equation and solving the resulting quadratic for $(t_r-t_e)$, one finds that

$$(t_r-t_e)=([(\mathbf{x}\cdot\mathbf{v})^2+(c_0^2-\mathbf{v}^2)\mathbf{x}^2]^{1/2}-\mathbf{x}\cdot\mathbf{v})/(c_0^2-\mathbf{v}^2), \tag{4}$$

and hence one can deduce the emission times corresponding to a set of equally spaced reception times.

In this way, one can simulate a sinusoidual signal, a band-limited random signal, or a signal from a rotating pressure pulse. The random signal is a superposition of densely packed sinusoids of random phase over the required frequency bandwidth. The rotating pressure pulse consists of a number of sources, spaced around the circumference of a circle, which move forward together; each of these is a superposition of a sine wave and its harmonics, phased to give a pulse at regular time intervals, and there is a time delay from each source to the next to give the impression of rotation. Furthermore, data from any of these different types of sources can be superposed.

This simulation capability has proved invaluable, both in checking for errors in the analysis programs and in understanding the behaviour of real data, and in sections 3.1 and 4.1 examples of how such signals have been analyzed will be given.

## 3. DE-DOPPLERIZATION

### 3.1. SIGNAL TO NOISE RATIO

Before proceeding to the analysis of real flyover data, one needs to consider the signal to noise ratio to be expected in the results.

The signal received at a microphone from a moving source (Mach number 0·3, altitude 300 ft) emitting band-limited random noise (1200 Hz to 1800 Hz) was simulated as described in section 2.4. The simulation was done three times, corresponding to sampling

the microphone output at 5 kHz, 10 kHz and 50 kHz, respectively. In all three cases, the subsequent de-Dopplerization analysis determined samples at a constant emission time sampling frequency of 5 kHz. As explained in section 2.1, this required interpolation between individual samples, and two simple ways of achieving this have been tested: for each calculated reception time, either the nearest available sample can be chosen or linear interpolation can be performed with use of one sample on either side.

Figure 4(a) shows that the crude method of choosing the nearest sample leads to a signal to noise ratio as low as 10 dB if the initial digitization rate and the final analysis sampling rate are equal. However, if the initial rate is increased by a factor of 2 or a factor of 10, then the signal to noise ratio improves to 18 dB or 33 dB, respectively (see Figures 4(b) and (c)). Linear interpolation offers a significant improvement on these figures: with ratios of initial to final sampling rates of 1, 2 and 10, the signal to noise ratios are 20 dB, 35 dB and 60 dB, respectively.

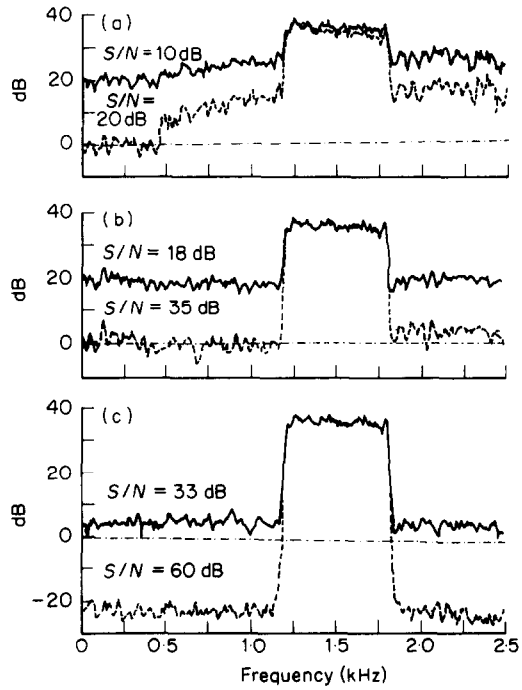


Figure 4. The effect of initial sampling rate on the signal to noise ($S/N$) ratio of a single microphone de-Dopplerized output. Band-limited random noise (1200 Hz to 1800 Hz) emitted by a moving source (Mach number 0·3, altitude 300 ft) was simulated. Initial sampling rate was (a) 5 kHz, (b) 10 kHz and (c) 50 kHz. Final analysis sampling rate was 5 kHz in all cases. ——, Nearest available sample chosen (no interpolation); - - -, linear interpolation between adjacent pair of samples. For comparison, a stationary source sampled with 12 bit accuracy would give 75 dB signal to noise ratio.

A sensible compromise would be to digitize initially at twice the analysis sampling rate, and to employ linear interpolation, giving a signal to noise ratio of about 35 dB. The signal to noise ratio for most FM tape recorders is typically 45 dB, and so there is little to be gained from a more stringent requirement. However, it is clear that linear interpolation is better than merely choosing the nearest sample; without it, one would have to sample the signal a further five times faster to achieve a comparable signal to noise ratio.

### 3.2. ANALYSIS OF BOEING 757 DATA

In this section data are presented from flyovers of a Boeing 757 aircraft powered by two Rolls-Royce RB211-535C engines. The results demonstrate how de-Dopplerization is necessary for identifying the tones in the spectrum of a high bypass ratio turbofan engine. Furthermore, it is now possible to calculate and plot the directivity of each tone.

Spectra from a ground level microphone were required with 400 equally spaced points up to 10 kHz and, following the recommendation of the last section, the recorded data were first digitized at 50 kHz. An anti-alias filter cutting off at 10 kHz was introduced, and for an approaching aircraft this slightly restricted the highest frequency available after de-Dopplerization. In the analysis a sampling rate of 25·6 kHz was used, with 1024 point fast Fourier transforms and a Hanning window, giving an effective noise bandwidth of 37·5 Hz. It would, of course, be possible to improve the resolution further, either by analyzing at a lower sampling rate or by taking more points in the transforms, but it must be remembered that the statistical accuracy is limited by the total flyover time.

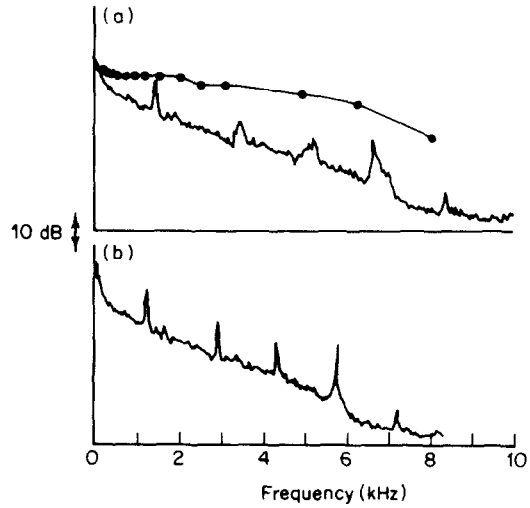


Figure 5. Narrow band spectra for Boeing 757, Run A (low approach, $N_L = 59\%$, 50° to engine intake, 20° angular average). (a) Before de-Dopplerization; (b) after de-Dopplerization. •——•, $\frac{1}{3}$ octave spectrum before de-Dopplerization.

Figures 5(a) and (b) show spectra from Run A (low approach, $N_L = 59\%$) at 50° to the engine intake, before and after de-Dopplerization, respectively. The angle to intake corresponds closely to the angle to flight direction. Until recently, only the $\frac{1}{3}$ octave levels plotted in Figure 5(a) would have been available, and these yield little information about the tonal content of the spectrum. Tones can, however, be seen in the narrow band spectrum, but they are blurred by the changing Doppler effect over a 20° angular averaging window and also Doppler-shifted to higher frequencies. The de-Dopplerized narrow band spectrum, on the other hand, has sharp tones which are now at the correct frequencies. There is a tone at 1250 Hz, which is unrelated to the engines, while the fan blade passing frequency (1F) (calculated as 1450 Hz) is not apparent. The second harmonic (2F), however, is seen clearly at 2900 Hz. The third harmonic (3F) at 4350 Hz is only 50 Hz above the expected blade passing frequency (4300 Hz) of the first stage of the IP compressor (1R1) and these two tones can just be distinguished. The large peak at 5750 Hz is the (1R1 + 1F) sum tone, although only 50 Hz below the expected 4F tone frequency.

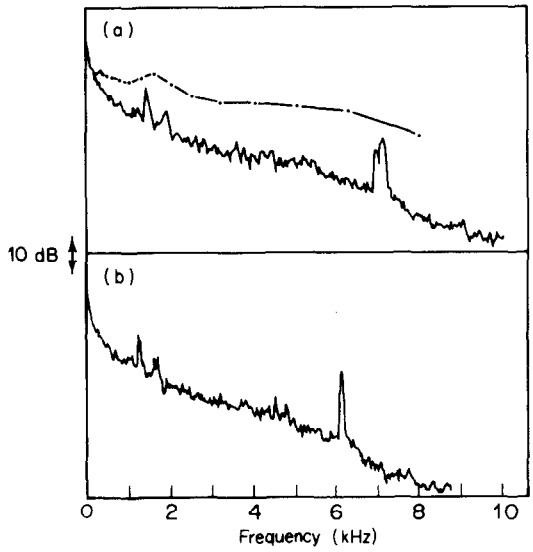


Figure 6. Narrow band spectra for Boeing 757, Run B (high approach, $N_L = 65\%$, 60° to engine intake, 10° angular average). (a) Before de-Dopplerization; (b) after de-Dopplerization. •——•, $\frac{1}{3}$ octave spectrum before de-Dopplerization.

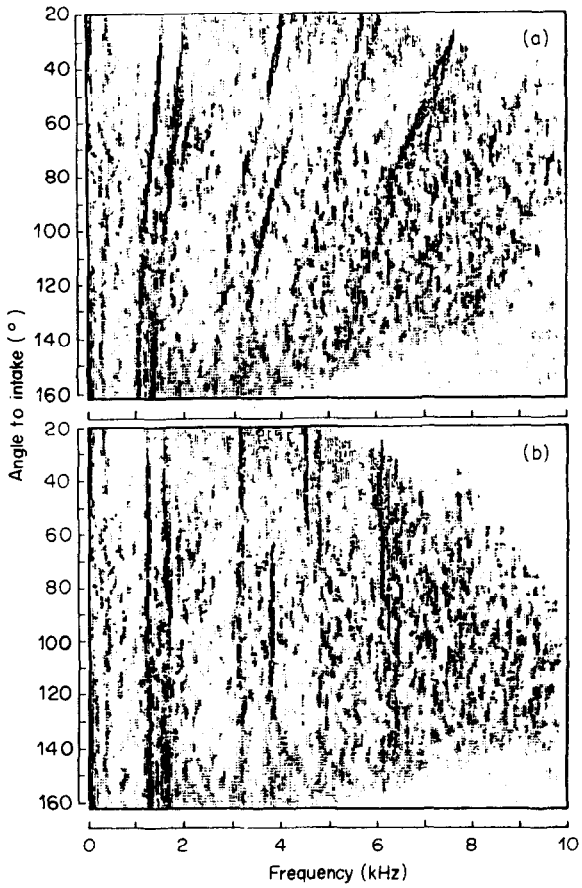


Figure 7. Density plots for Boeing 757, Run B. The darkness indicates tone protrusion. (a) Before de-Dopplerization; (b) after de-Dopplerization.

Spectra for Run B (high approach, $N_L = 65\%$) at 60° to the engine intake, with a 10° averaging window, are shown in Figures 6(a) and (b). As before, the spectra in Figure 6(a) are misleading, and for example one might wrongly conclude that there are two tones at around 7000 Hz. De-Dopplerization again greatly improves the spectrum. The fan blade passing frequency (1F) is now apparent at 1600 Hz, and this time the 1R1 tone (4530 Hz) and the 3F tone (4800 Hz) are separated by 270 Hz and are, therefore, well resolved. Likewise the (1R1 + 1F) tone (6130 Hz) and the 4F tone (6400 Hz) are well separated: the former is a large sum tone, while the latter is barely present at all.

Figure 7(a) and (b) show density plots for Run B. These have the advantage that an entire flyover can be presented on a single graph, the darkness indicating the tone protrusion as a function of angle and frequency. There are now only 200 points up to 10 kHz, and a 5° averaging window was used at 1° intervals. The resolution of these density plots is the best that can be achieved with the spectra available, but they do provide a valuable check on the accuracy of de-Dopplerization and give a crude idea of field shape for each tone.

A more accurate indication of some de-Dopplerized field shapes for Run B is provided by Figures 8(a)-(c). These are at three different frequencies, $1\frac{1}{2}$F, 2F and (1R1 + 1F), respectively, the first of which is intended to indicate the broad band noise level.

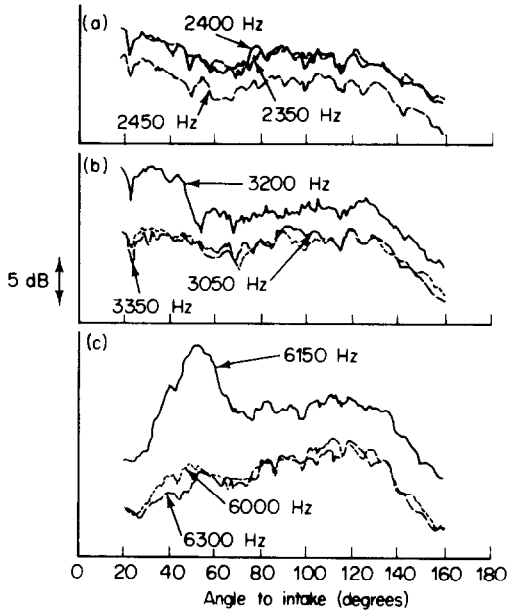


Figure 8. De-Dopplerized field shapes for Boeing 757, Run B (corrected for spherical spreading effect to constant distance). (a) $1\frac{1}{2}$F (indicating broad band field shape); (b) 2F; (c) 1R1 + 1F. In each case, field shapes for the broad band noise on either side of the selected frequency are also plotted.

All these results demonstrate that de-Dopplerized narrow band spectra can give clear definition of engine tones, whereas previously the spectra were of a comparatively broad band character. Furthermore, the density plots and field shapes have shown how the technique allows one to follow the level of each tone as a function of angle.

### 3.3. ANALYSIS OF AVRO SHACKLETON DATA

De-Dopplerization has also been applied to flyovers of an Avro Shackleton, an aircraft with four Rolls-Royce Griffon engines, each driving a set of counter-rotating propellers.

In view of the current interest in propellers, it is particularly interesting to gain accurate information on the tonal content of the noise from such an aircraft.

Figure 9 shows the narrowband spectra at 90°, between 500 Hz and 1000 Hz, before and after de-Dopplerization, for an angular average of 10°. At this angle, the tones are blurred

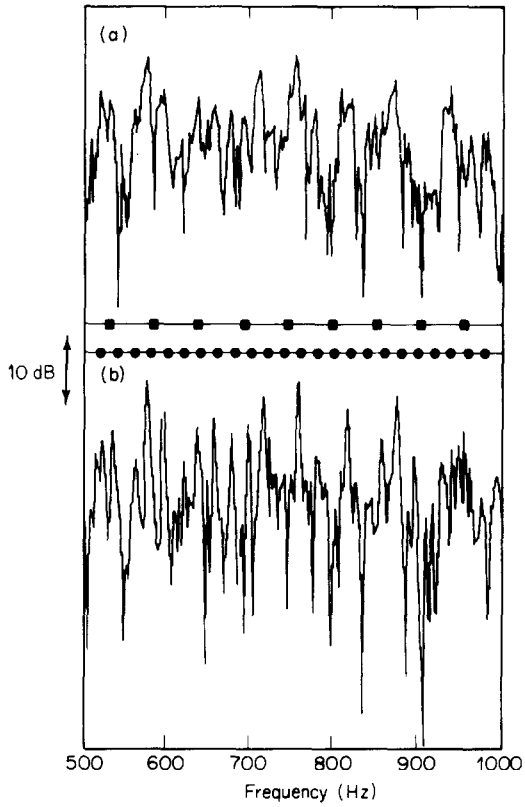


Figure 9. Upper half of narrow band spectra for Avro Shackleton (2400 rpm, 90° to flight direction, 10° angular average). (a) Before de-Dopplerization; (b) after de-Dopplerization. ■—■, Harmonics of propeller blade passing frequency (fundamental, 53·1 Hz); ●—●, harmonics of half engine rotational speed (fundamental, 20 Hz).

by the changing Doppler effect, but their frequencies are not significantly shifted. The analysis was performed to give 400 points up to 1 kHz, each separated by 2·5 Hz. The engines were four-stroke, running at 2400 rpm, and hence the spectrum is dominated by half engine orders every 20 Hz. These are clearly resolved in the de-Dopplerized spectrum, even up to $24\frac{1}{2}$ engine orders at 980 Hz. Blade passing frequency is 53·1 Hz, since each propeller has three blades and the gearing ratio is 0·4423. Certain harmonics of this frequency are clearly seen over the spectrum (up to the 17th harmonic), in spite of the engine tones. The power of the technique for these closely spaced tones is especially apparent at the higher end of the spectrum: with a linear frequency scale, the blurring effect of source motion increases with frequency, but this is completely eliminated by de-Dopplerization.

Field shapes at blade passing frequency for two flyovers are shown in Figure 10(a) and (b). In the first of these, the four engines were unsynchronized (but note that the two propellers on each engine always remain locked in phase), and the lobular pattern was probably due to the changing relative phase of the engines. In the second case, the

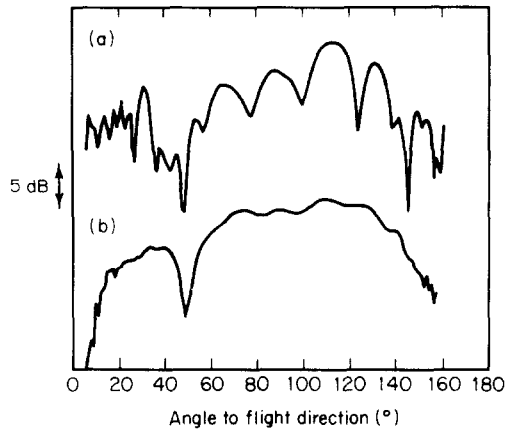


Figure 10. De-Dopplerized field shapes for Avro Shackleton (corrected for spherical spreading effect to constant distance), at propeller blade passing frequency. (a) Unsychronized engines; (b) synchronized engines.

engines were synchronized, and the interference between engines disappears, although the trough between 40° and 50° remains.

Finally, Figure 11 shows the complete de-Dopplerized spectrum at 90° to the flight direction. This time, however, the angular average is over 90°, and this has two advantages.

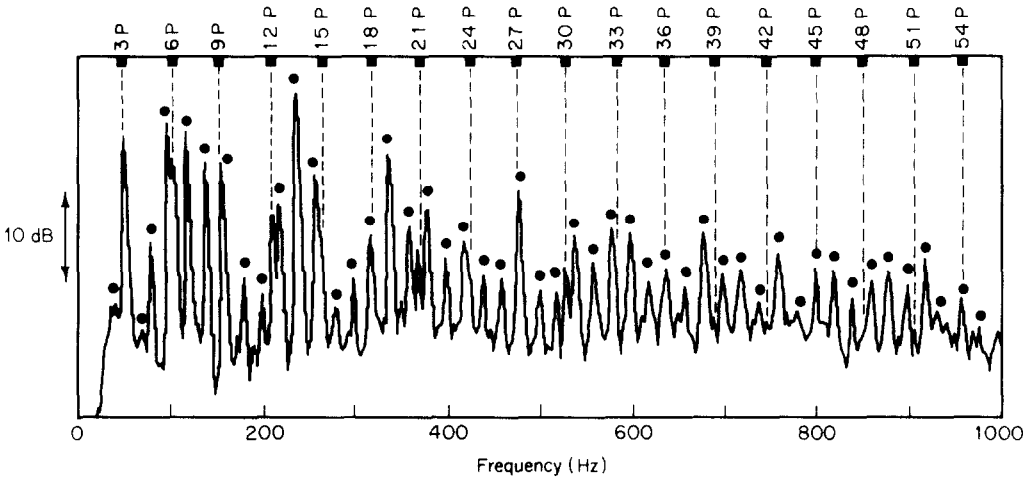


Figure 11. De-Dopplerized narrow band spectrum for Avro Shackleton (2400 rpm, 90° to flight direction, 90° angular average). ■, Harmonics of propeller blade passing frequency (fundamental, 3P, 53·1 Hz); ●, harmonics of half engine rotational speed (fundamental 20 Hz).

The first is that the broad band noise level between tones, which is fairly constant with angle, is estimated more accurately with a longer averaging time; this is seen clearly when this figure is compared with Figure 9. Secondly, since most of the sound power from the propellers is emitted into the sector between 45° and 135° to the flight path, Figure 11 can be considered as a good indication of the sound power level of the source as a function of frequency.

De-Dopplerization is therefore of great value in analyzing the noise from propeller driven aircraft. Tones across the whole spectrum can be resolved, and their relative levels assessed, and field shapes for specified tones, even high harmonics, can be plotted.

Furthermore, a wide angular average yields an accurate estimation of the broadband noise level, as well as giving a good indication of the sound power level of the source as a function of frequency.

## 4. ACOUSTIC IMAGING

In section 3 we examined the output from a single de-Dopplerized microphone channel, and saw how it was especially helpful in identifying tones in a spectrum. We now illustrate some of the effects of summing several such signals in parallel from an array of microphones, thus providing source images. In this case, we concentrate rather more on the broad band content of the spectra analyzed.

### 4.1. RESPONSE TO SIMULATED BAND-LIMITED RANDOM NOISE

Figure 12 shows the response of a four-microphone longitudinal array to simulated band-limited random noise (Mach number 0·3, altitude 300 ft, microphone spacing 10 ft). It is presented as a longitudinal scan (i.e., in the direction of flight), covering 60 ft behind and 60 ft in front of the true source position, at a frequency of 1504 Hz (frequency band separation 19·5 Hz).

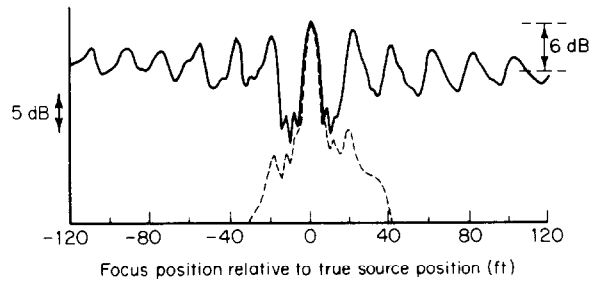


Figure 12. Acoustic image of a simulated moving point source (Mach number 0·3, altitude 300 ft), analysis at 1504 Hz with use of a 4-microphone array (spacing 10 ft). ——, Band-limited random noise; - - -, 1500 Hz sinusoid.

At first sight, the response resembles that of the static acoustic telescope, with aliases in both directions. However, there is an important difference, in that the alias images are now due to completely uncorrelated components of the source: those in front of the true source position were emitted at lower frequencies, while those behind were emitted at higher frequencies. In addition, the degree of correlation between the outputs of the individual microphones will reduce as the focus position moves further out in either direction, and the peaks and troughs begin to smooth out at a level which is the sum of four uncorrelated components (6 dB below the peak). This is because the de-Dopplerization is inaccurate away from the true source position, and the outputs of any two microphones will not be correctly aligned over the whole averaging time used. In practice, the fall in coherence can be quite marked, and this is put to advantage in the next section.

For comparison, the response to a 1500 Hz sinusoid, simulated under the same conditions, is also shown in Figure 12. As expected, there are no significant aliases in this frequency band: aliases in front of the true source position would occur at higher frequencies, and those behind would be at lower frequencies.

In any attempt at interpreting the image of a moving source, as is done in the static case [7], one must therefore take account of how the source is distributed in frequency as well as in space.

### 4.2. LOCKHEED TRISTAR: LONGITUDINAL SCAN

A longitudinal scan (i.e., in the flight direction) from a flyover of a Lockheed TriStar aircraft, at 600 ft altitude and 360 ft/s speed, is shown in Figure 13. The frequency band chosen includes the fan blade passing frequency. There were four microphones, each separated by 12·5 ft, and the results are averaged between 40° and 50° to the engine intake.

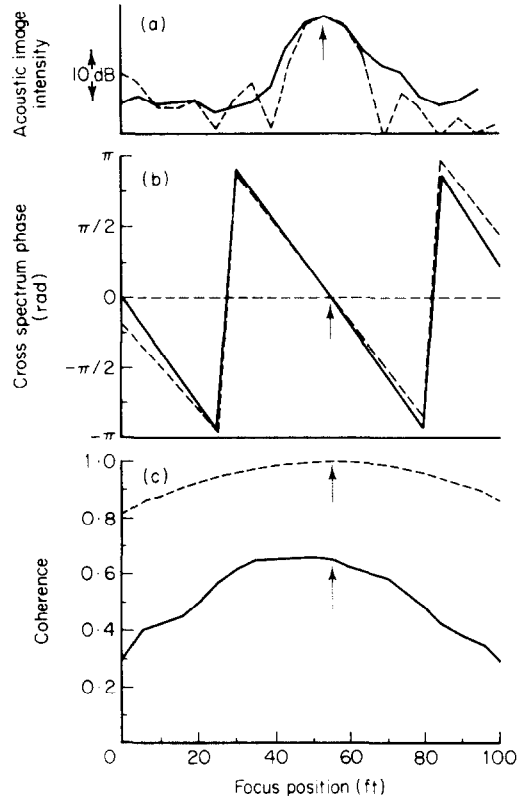


Figure 13. Longitudinal scan for a Lockheed TriStar flyover (Mach number 0·32, altitude 600 ft), with use of a 4-microphone array (spacing 12·5 ft). (a) Acoustic image intensity; (b) phase of cross spectrum between de-Dopplerized outputs of microphones 2 and 3; (c) coherence between de-Dopplerized outputs of microphones 2 and 3. ——, Actual data; - - -, simulated data. The arrow indicates the zero phase position.

The central engine was at flight idle, and so all the engine noise was emitted from approximately the same longitudinal position. In addition to the summed de-Dopplerized outputs from all the microphones, the (unsmoothed) phase of the cross spectrum and the coherence between two of them are also displayed. Furthermore, for comparison, we show the results of simulating the source and flight conditions as accurately as possible.

Alias images will occur whenever the relative phase between two outputs is zero, so that reinforcement occurs. In practice, however, the coherence reduces rapidly on each side of the true source position, as discussed in the last section; this can now be put to advantage in accurately locating a moving source, simply by looking for the position of zero phase and maximum coherence.

The simulated results show remarkably good agreement, especially for the relative phase between two microphones, showing how accurately the phase can be determined

from experimental data. Agreement for the coherence is not so good, but one would generally expect less coherence in experimental data.

### 4.3. LOCKHEED TRISTAR: TRANSVERSE SCAN

Figure 14 shows two transverse scans (perpendicular to the flyover plane) of the Lockheed TriStar during the same flyover, with use of a 16-microphone array. At both

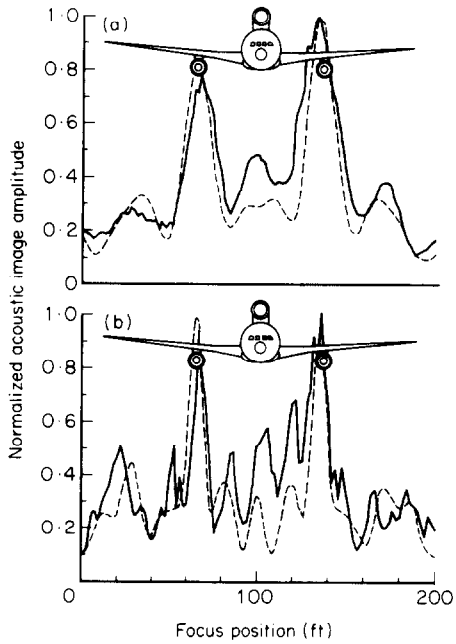


Figure 14. Tranverse scans for a Lockheed TriStar flyover (Mach number 0·32, altitude 600 ft), with use of a two-dimensional 16-microphone array, showing images of the two wing-mounted engines (central engine at idle). (a) 800 Hz; (b) 1600 Hz. ——, Actual data; - - -, simulated data.

frequencies shown, the two positions of maximum response are clearly seen, corresponding to the two-wing-mounted engines (the central engine was at flight idle). Simulated scans were again performed, and these reproduce the same general character at each frequency; the positions and relative heights of sidelobe peaks depend on the separation of the two sources and the response characteristics of the microphone array, which in this case was not symmetric.

Not only do these scans graphically illustrate the capability of flyover acoustic imaging, therefore, but they also clearly demonstrate the value of source simulation. This can be carried out in advance of a flyover test with the aim of designing a microphone array with the best characteristics for the particular sources to be studied.

## 5. CONCLUSIONS

A technique for eliminating the Doppler effect from aircraft flyover measurements has been developed and tested on a variety of different aircraft. Acoustic imaging, an extension of de-Dopplerization, has also been convincingly demonstrated.

Details of both processes have been provided in the paper, which also shows how they are achieved in practice. This includes a description of how to simulate aircraft flyover

noise measurements, and this has proved invaluable, both in checking for errors in the analysis programs and in understanding the behaviour of real data.

Analysis of simulated data has shown that a signal to noise ratio of 35 dB can be achieved by digitizing initially at twice the analysis sampling rate, and then employing linear interpolation between samples. The results from the Boeing 757 data have demonstrated how de-Dopplerized narrow band spectra can give clear definition of the tones from a high bypass ratio turbofan engine, whereas previously the measured spectra were of a comparatively broad band character. In addition, the closely spaced engine and propeller tones from the Avro Shackleton can be clearly resolved, and some interesting field shapes for counter-rotating propellers have been revealed.

The capability of acoustic imaging has been clearly illustrated by longitudinal and transverse scans for a Lockheed TriStar flyover. These results show how accurately the relative phase between two microphones can be determined from experimental data, and they also demonstrate the value of simulation. For example, a microphone array can be designed in advance of a flyover test with the best characteristics for the particular sources to be studied. Simulation has also shown how any attempts at interpreting the image of a moving source must take account of how the source is distributed in frequency as well as in space; the acoustic images illustrated in this paper have started to pave the way towards in-flight noise source breakdown, as is done routinely for static engines.

## ACKNOWLEDGMENTS

The authors are particularly grateful to Dr. M. A. Swinbanks (MAS Research Limited) and Mr. M. G. Smith, who assisted in developing the techniques described in this paper. They also acknowledge the benefit of discussions with their colleagues, especially Dr. B. J. Tester, Dr. M. J. Fisher, Dr. A. J. Kempton, Dr. V. M. Szewczyk and Dr. M. J. Pye. The results relating to the Boeing 757 aircraft are published with the kind permission of The Boeing Company. Finally, the authors would like to thank the Directors of Rolls-Royce Limited for permission to publish this paper.

## REFERENCES

1. D. ROY 1984 *AIAA/NASA Paper No.* 84-2354. Doppler frequency shift for aircraft noise in a refractive atmosphere.
2. H. P. VERHAS 1983 *Journal of Sound and Vibration* **89**, 487-497. A restoration procedure for (non-stationary) signals from moving sources.
3. A. W. MUELLER and J. S. PREISSER 1981 *NASA TP* 1898. Flight test of a pure-tone acoustic source.
4. J. S. PREISSER and D. CHESTNUTT 1984 *Journal of Aircraft* **21**, 453-461. Flight effects on fan noise with static and wind-tunnel comparisons.
5. D. GRIDLEY 1982 *NASA CR* 165867. Program for narrow-band analysis of aircraft flyover noise using ensemble averaging techniques.
6. J. BILLINGSLEY and R. KINNS 1976 *Journal of Sound and Vibration* **48**, 485-510. The acoustic telescope.
7. B. J. TESTER and M. J. FISHER 1981 *American Institute of Aeronautics and Astronautics Paper No.* 81-2040. Engine noise source breakdown: theory, simulation and results.